The Illinois Roadway Simulator: A Mechatronic Testbed for Vehicle Dynamics and Control

Sean Brennan and Andrew Alleyne, *Member, IEEE*

***Abstract*—The Illinois Roadway Simulator (IRS) is a novel, mechatronic, scaled testbed used to study vehicle dynamics and controls. An overview of this system is presented, and individual hardware issues are addressed. System modeling results on the vehicles and hardware are introduced, and comparisons of the resulting dynamics are made with full-sized vehicles. To address the realism factor of using scaled vehicles, comparisons are made between dynamic responses of full-scale and IRS-scale vehicles. The method of *dynamic similitude* is a key to gaining confidence in the scaled testbed as an accurate representation of actual vehicles to a first approximation. The IRS is then used in a vehicle control case study to demonstrate the potential benefits of scaled investigations. The idea of driver-assisted control is formulated as a yaw-rate model-following problem based on the representation of the driver as a known disturbance model. The controller is designed and implemented to show that the vehicle's dynamics can be changed to match a prescribed reference model.**

***Index Terms*—Dynamic similitude, mechatronics, road vehicle control, scaling.**

I. Introduction

THE use of mechatronic systems in vehicles has increased dramatically in the past two decades, thereby increasing the safety, performance, and reliability of cars and trucks on the road. Additionally, the projected use of on-board control and diagnostic systems is certain to increase in the future [1]. Both governmental regulations and consumer demand drive this increase. While a great deal of the mechatronic systems have focused on vehicle power trains and related emissions, a significant amount of research has been done on the control of vehicle dynamics. This includes robust approaches to vehicle safety [2], active vehicle suspensions [3], and vehicle over/understeer control [4], [5]. The interested reader is referred to the survey articles [6] and [7] for many additional references on vehicle control.

Much of the vehicle control work to date has been limited to simulation because the use of a full-size vehicle to test controllers is often prohibitively expensive as well as dangerous. The focus of the research presented in this paper has been to develop a scale version of a vehicle and a roadway for safe and economic testing of controller strategies: the Illinois Roadway Simulator (IRS). Previous investigations using scaled vehicles [8], [9] have mostly involved moving the vehicles along some fixed surface. This may incur a host of interfacing and sensing issues. The IRS is an experimental testbed consisting of scaled vehicles, running on a simulated road surface, where the vehicles are held fixed with respect to inertial space and the road surface moves relative to the vehicle. The analogy would be wind-tunnel testing of aerospace systems.

There are several advantages of the IRS over full-scale vehicle testing. First, the availability of scale components makes construction faster and cheaper. The durability of these vehicles and the ability to intervene during an accident make testing safe and repeatable. The scheduling and use of public or private roadways is not an issue. No drivers or pedestrians are put at risk during testing of aggressive vehicle controllers. The simulated roadway surface can be varied quickly and easily to simulate changing road surfaces. Finally, testing has shown a great deal of dynamic similitude between scale and full size vehicles.

The remainder of the paper develops as follows. In Section II, an overview and more detailed description of the IRS system is given. Section III presents dynamic models of the IRS system, along with experimental results to verify the models. Section III also includes models and experimental results for individual vehicles, including a detailed comparison between scaled and full-size vehicles based on dynamic similitude and the *Buckingham Pi* theorem. In Section IV, a yaw-rate vehicle control approach is given to illustrate the type of investigations that can be done with the IRS. Section V summarizes the main points of the paper.

II. IRS Overview

The IRS's scaled roadway surface consists of a 4 ft $\times$ 8 ft treadmill capable of top speeds of 15 mi/h. Scale vehicles are run on the treadmill via multiple wall-mounted transmitter systems operating between 50–100 MHz. The remainder of the IRS consists of a driver console, digital-signal-processor (DSP) and PC-based interface computers, A/D and D/A converters, a significant amount of electronic interface equipment, several separate receiver systems, a vehicle position sensor system, and the vehicles. The vehicle controller hardware loop uses a reference signal that can come either indirectly via the manual driver console or directly from a computer-generated signal. If the signal is from the manual driver console it is first input to a computer via an Analog Devices RTI-815 Analog I/O board sampling at 1 kHz. The computer then outputs analog voltage commands, via an Analog Devices RTI 802 Analog Output board, to the vehicle's transmitter. This voltage signal is then converted to a FM signal. The receiver system on the vehicle transforms the transmitter's FM signals into pulsewidth modulated signals, which are then sent to the vehicle actuators. Each actuator has a built-in analog controller that converts the pulsewidth-modulated signals into reference commands.

Manuscript received September 18, 1998; revised August 27, 1999. Recommended by Technical Editor H. Peng.

The authors are with the Department of Mechanical and Industrial Engineering, University of Illinois, Urbana-Champaign, Urbana, IL 61801 USA (e-mail: alleyne@uiuc.edu).

Publisher Item Identifier S 1083-4435(00)11063-4.

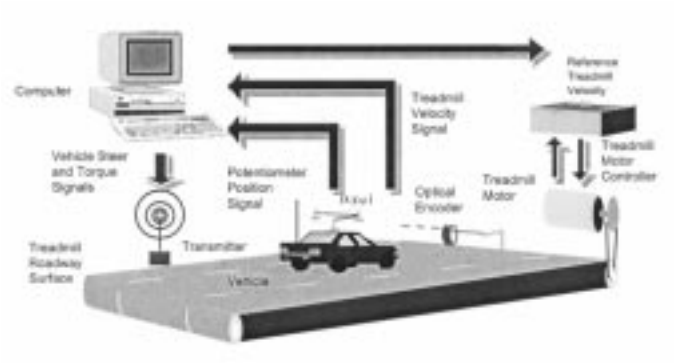

Fig. 1. IRS system schematic.

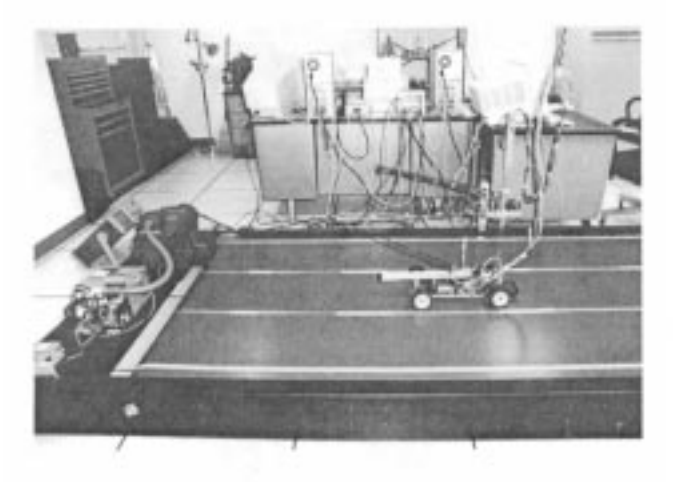

Fig. 2. IRS system.

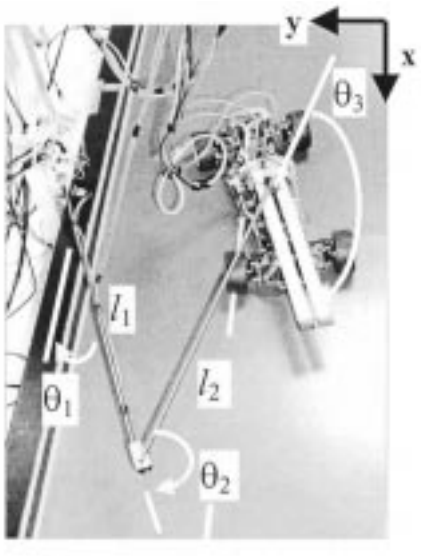

Fig. 3. Sensor arm.

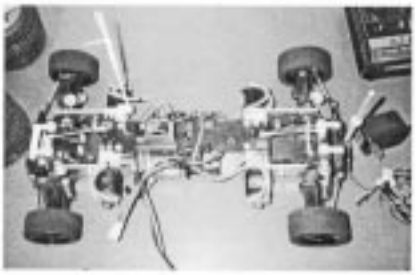

Fig. 4. IRS vehicle.

The treadmill road surface servos the vehicle position with respect to an inertial reference point. The roadway speed is monitored via an optical encoder. To maintain the vehicle on the treadmill, a separate computer uses the vehicle's inertial position as feedback and sends an output voltage signal to the treadmill. The treadmill uses an industrial motor controller that converts the input voltage level to a reference speed, and adjusts the dc drive motor current to match this speed accordingly. Figs. 1 and 2 give a representation of the entire system.

As designed, the treadmill does not allow speed reversing. Hence, acceleration of the treadmill is accomplished by a dc motor that applies torque to the treadmill belt, while deceleration is accomplished by allowing friction to slow the treadmill down. A detailed description of the treadmill dynamics may be found in [10].

The vehicle control feedback loop begins with a position sensor connecting the vehicle with a known inertial reference point. The sensor consists of a three-bar linkage with encoders at each joint. The joint angles are then used to determine the position and orientation of the vehicle on the treadmill. Fig. 3 shows a sensor arm, as well as the angle and length conventions used to determine vehicle position.

The corresponding vehicle coordinates are given as

$$\begin{aligned} x &= l_1 \cdot \cos\theta_1 + l_2 \cdot \cos(\theta_1 + \theta_2) \\ y &= l_1 \cdot \sin\theta_1 + l_2 \cdot \sin(\theta_1 + \theta_2) \\ \psi &= (\theta_1 - \theta_{1o}) + (\theta_2 - \theta_{2o}) + (\theta_3 - \theta_{3o}) \end{aligned} \tag{1}$$

where

l_1, l_2	link lengths;
$\theta_1, \theta_2, \theta_3$	joint rotations;
$\theta_{1o}, \theta_{2o}, \theta_{3o}$	reference positions calibrated to inertial space.

Initial experiments used potentiometers for the joint angle sensors to enhance system mechanical robustness. However, after several experimental design iterations, high-resolution encoders are currently being used for their linearity and resistance to wear. Custom-mounted brackets were designed so that the encoders themselves saw no side loading.

There are several vehicles in use on the IRS, each with different operating capabilities. They range from a simple 2WD front steer vehicle to a 4WS vehicle with independent drive motors for each wheel, shown in Fig. 4.

Commercial off-the-shelf (COTS) transmitter systems were used to send signals to the on-board motor and steer servo controllers. This communication system induced a time delay in the control loop. The COTS system was retained in the control loop because of the simplicity involved with interfacing the transmitters which used potentiometers to generate analog control signals. It is possible to directly interface the on-vehicle controllers and this will reduce or eliminate the delay. However, this will greatly increase the system complexity.

All data acquisition and control features are handled via Wincon, a Windows-based control program that runs real-time

code generated by Matlab/Simulink's Real Time Workshop toolbox. Custom drivers were written in C to communicate with the Analog Devices boards. This Wincon interface eliminated lower level C-programming and allowed all functions to be handled with a GUI type of Simulink interface. Additionally, it provided for real-time viewing of data.

III. Vehicle System Modeling

A. Vehicle Dynamics

The well-known bicycle model [11] was taken as an initial estimate for the dynamics of the scaled IRS vehicle. The bicycle model assumes a constant longitudinal velocity of the vehicle and consists of two dynamic degrees of freedom: lateral velocity and yaw rate. The state-space formulation [12] is as follows:

$$\frac{\partial}{\partial t}\begin{bmatrix} Y \\ \partial Y/\partial t \\ \psi \\ \partial \psi/\partial t \end{bmatrix} = \begin{bmatrix} 0 & 1 & 0 & 0 \\ 0 & \frac{A_1}{V} & -A_1 & \frac{A_2}{V} \\ 0 & 0 & 0 & 1 \\ 0 & \frac{A_3}{V} & -A_3 & \frac{A_4}{V} \end{bmatrix} \cdot \begin{bmatrix} Y \\ \partial Y/\partial t \\ \psi \\ \partial \psi/\partial t \end{bmatrix} + \begin{bmatrix} 0 & 0 \\ B_1 & B_2 \\ 0 & 0 \\ B_3 & B_4 \end{bmatrix} \begin{bmatrix} \delta_f \\ \delta_r \end{bmatrix} \tag{2}$$

where

$$A_1 = \frac{-(C_{\alpha f} + C_{\alpha r})}{m}$$
$$A_2 = \frac{(C_{\alpha r} \cdot L_2 - C_{\alpha f} \cdot L_1)}{m}$$
$$B_1 = \frac{C_{\alpha f}}{m}$$
$$B_2 = \frac{C_{\alpha r}}{m},$$
$$A_3 = \frac{(C_{\alpha r} \cdot L_2 - C_{\alpha f} \cdot L_1)}{I_z},$$
$$A_4 = \frac{-(C_{\alpha f} \cdot L_1^2 + C_{\alpha r} \cdot L_2^2)}{I_z}$$
$$B_3 = \frac{L_1 \cdot C_{\alpha f}}{I_z},$$
$$B_4 = \frac{-L_2 \cdot C_{\alpha r}}{I_z}$$

and

m	mass of the vehicle;
I_z	vehicle inertia about vertical axis at the C.G.;
V	vehicle forward velocity;
$C_{\alpha f}$, $C_{\alpha r}$	front, rear cornering stiffnesses;
L	$= L_1 + L_2$;
δ_f, δ_r	front, rear steering angle;
ψ	yaw angle;
Y	lateral position relative to some reference.

From (2), the input–output transfer function from front input steer angle to yaw rate is given as

$$\frac{\dot{\psi}(s)}{\delta_f(s)} = \frac{C_{\alpha f} V^2 m L_1 s + C_{\alpha f} C_{\alpha r} L V}{a_1 s^2 + a_2 s + a_3} \tag{3}$$

and from rear input steer angle to yaw rate is

$$\frac{\dot{\psi}(s)}{\delta_r(s)} = \frac{-C_{\alpha r} V^2 m L_2 s - C_{\alpha f} C_{\alpha r} L V}{a_1 s^2 + a_2 s + a_3} \tag{4}$$

with

$$a_1 = I_z m V^2$$
$$a_2 = V(I_z(C_{\alpha f} + C_{\alpha r}) + m(C_{\alpha f} L_1^2 + C_{\alpha r} L_2^2))$$
$$a_3 = C_{\alpha f} C_{\alpha r} L^2 - m V^2 (C_{\alpha f} L_1 - C_{\alpha r} L_2).$$

We can note that the above equations consist of many values that are experimentally measurable, such as vehicle speed, mass, and moment of inertia. If these values are measured and substituted into the transfer function given above, then a reasonable approximation of the vehicle's transfer function should be obtained. Although the measurement of the vehicle mass is trivial, measuring the other values is not intuitively obvious.

The vehicle's mass was determined simply by weighing it on a standard balance scale. The center of gravity was determined by balancing the vehicle and determining the location where zero net gravitational moment acted. To determine the z-axis moment of inertia, the vehicle was suspended by a torsional spring and the period of oscillation about the z axis was measured. For a mass that is suspended by a spring whose force is proportional to angle, the governing equation is given as

$$\sum M_z = I_z \ddot{\theta} = -\beta \dot{\theta} - k\theta \tag{5}$$

where β is a damping term (N·m·s/rad), I_z is the z-axis moment of inertia (kg·m^2), and k is a spring constant (N·m/rad). Taking the Laplace transform of the equation gives the characteristic equation

$$I_z s^2 + \beta s + k = 0. \tag{6}$$

Solving for the roots of the characteristic equation results in the eigenvalues

$$s = -\frac{\beta}{2I_z} \pm \sqrt{\left(\frac{\beta}{2I_z}\right)^2 - \frac{k}{I_z}}. \tag{7}$$

If the system is underdamped, we can measure the exponential decay term $-\beta/(2 * I_z) = \lambda$, as well as the spring constant k and the frequency of the response. From these measurements, we note that

$$I_z = \frac{k}{\lambda^2 + \omega^2}. \tag{8}$$

Fig. 5 shows a sample of the time response, as well as the exponential fit to determine λ. For this figure, λ is approximately 0.051 rad/s and the frequency of the system can be identified as 0.965 rad/s. Using the equation above, the moment of inertia for this particular case is calculated to be 0.0730 kg·m^2.

To determine the cornering stiffness of the tires, the special test rig shown in Fig. 6 was devised. With this test stand it is possible to control both the slip angle and the normal force on each tire. Fig. 7 shows the results of testing a particular scale tire at three different normal loads. By determining the tangent line at zero slip angle it is possible to determine the actual cornering stiffness for the tire. The cornering stiffness characteristics will

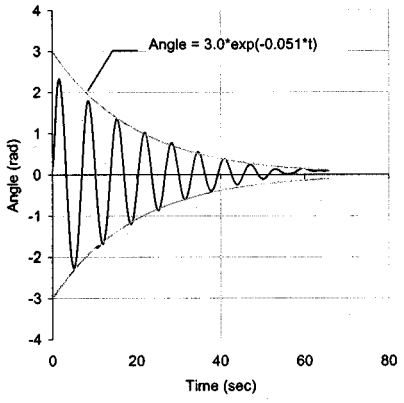

Fig. 5. Time response for I_z test.

Fig. 6. C_α testing stand.

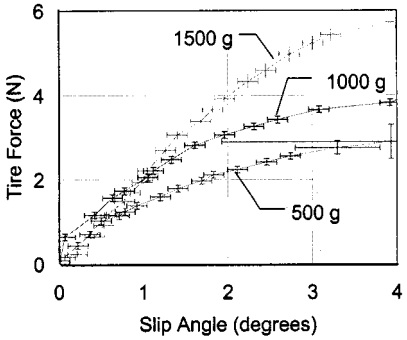

Fig. 7. Lateral tire forces.

change with tire type. Fig. 8 shows the cornering stiffness determined for a low and high C_α tire. A summary of measured parameters is given in Table I for three different IRS vehicles.

Although the system of (5) uses the steer angle as the input, for the IRS system the dynamics of Fig. 9 occur between the voltage steer command and the actual steer angle. There is a communication time delay of 15 ms from the D/A computer signal to the actuator's reference signal. The steer actuator is an electric motor controlled by an analog feedback device. The rate limit occurs due to the gearing in the motor necessary for sufficient output torque. Similar rate-limited steer-actuator effects can be seen in actual vehicles responses, e.g., limited flow-rate systems in hydraulic power-steering units [13].

Fig. 10 shows the time- and frequency-domain characteristics of steer servos used on the IRS vehicles. The responses are given

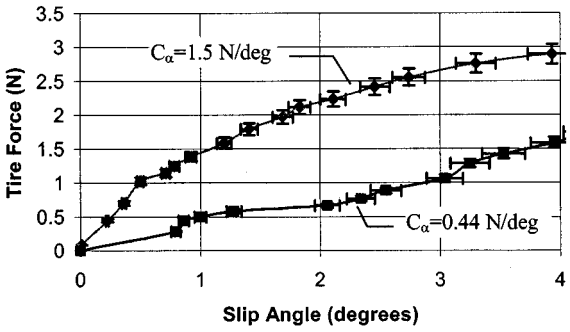

Fig. 8. Lateral tire forces.

TABLE I
IRS VEHICLE PARAMETERS

	Vehicle #1	Vehicle #2	Vehicle #3
M	1.47 kg	4.025 kg	2.33 kg
I_z	0.024 kg m^2	0.12 kg m^2	0.052 kg m^2
L_1	0.13 m	0.139 m	0.18 m
L_2	0.15 m	0.189 m	0.18 m
$C_{\alpha 1}$	1.53 N/deg.	0.53 N/deg.	1.53 N/deg.
$C_{\alpha 2}$	1.53 N/deg.	0.53 N/deg.	1.53 N/deg.

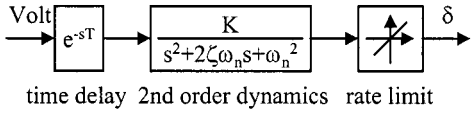

Fig. 9. Steer actuator dynamics.

at several different operating amplitudes while the servos are unattached to any vehicle. The approximate bandwidth is 8 Hz. When using the servo installed in Vehicle #2, transfer functions approximations for the front and rear steering are

$$\frac{\delta_f(s)}{V_f(s)} = \frac{3510}{s^2 + 60.5 \cdot s + 1764} \left[\frac{\text{rad}}{\text{V}}\right] \tag{9}$$

$$\frac{\delta_r(s)}{V_r(s)} = \frac{751}{s^2 + 36 \cdot s + 625} \left[\frac{\text{rad}}{\text{V}}\right]. \tag{10}$$

Although the actual servo motors are the same for the front and rear steering, the linkages between the steer servos and the wheel angles are different. As a result of the different increases in effective inertia, the dynamics for the two transfer functions are different.

B. Experimental Verification

In this section, we examine the accuracy of the parameters identified in Section III. Fig. 11 shows the frequency response of the entire vehicle from front steer input to yaw rate at a forward velocity of 3.0 m/s. Experimental frequency responses are compared with a transfer function obtained by directly substituting the identified parameters for Vehicle #2 along with the fast steer servo model of Fig. 10 and the communication time delay.

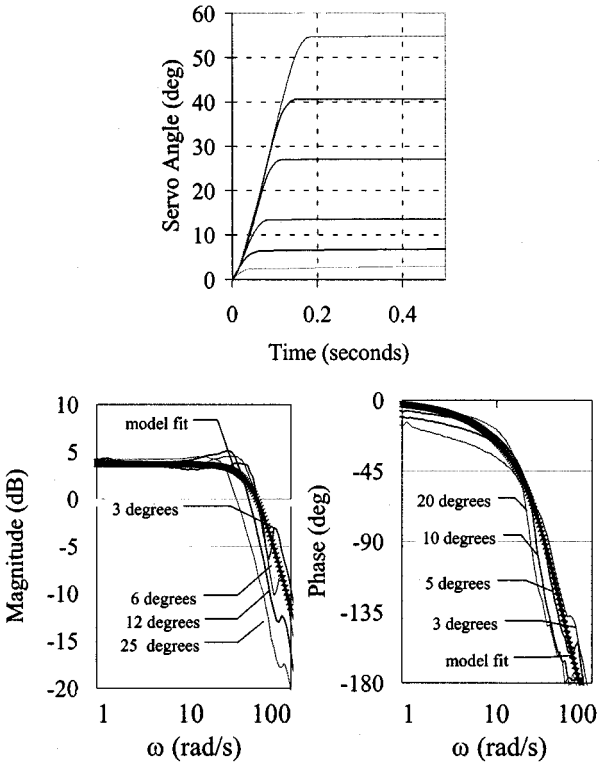

Fig. 10. Steer dynamics: time and frequency domain.

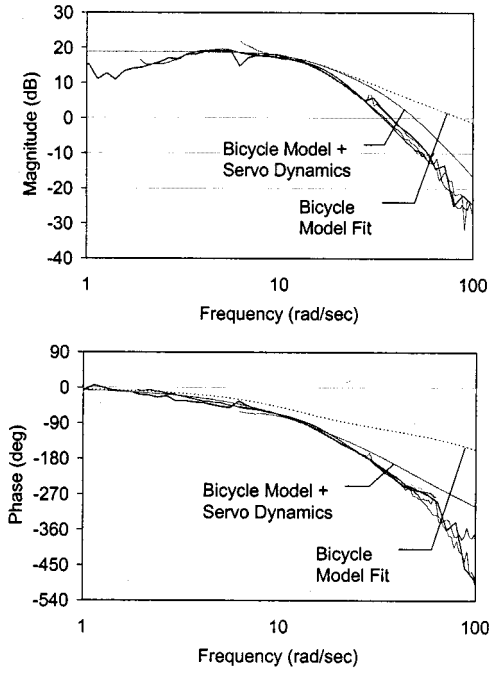

Fig. 11. Frequency-domain model comparisons for front steering.

Similar results are obtained for a frequency response of the entire vehicle from rear steer input to yaw rate. Section IV shows the $\dot{\psi}$ time response of the vehicle for a series of steer inputs. As can be seen in the figure, as well as in Section IV, the fits in both the time and frequency domain are good. The fit could be made even better since the steer servo was identified while the vehicle was not actually running on the IRS and the vehicle's inertia and mass were not measured with the sensor arm attached. By slightly tuning transfer function coefficients, the results of Fig. 11 could be actually be improved. However, these results already validate the direct use of the offline parameter identification in the beginning of this section. The results also provide confidence in discussing the following dynamic similitude comparison of the IRS scaled vehicles with full-size vehicles.

C. Dynamic Similitude Analysis

If a solution to the differential equations in (5) for the IRS vehicles exists, then the vehicle yaw degree of freedom will be a function dependent on the scaled parameters

$$\psi = f(\delta, m, I_z, V, L_1, L_2, C_{\alpha f}, C_{\alpha r}, t). \tag{11}$$

The *Buckingham Pi* theorem [14] states that any function that can be written in the above form can be rewritten in a dimensionless form without changing the solution to the differential equation. This rewriting is achieved by grouping the parameters into (n–m) independent dimensionless parameters, where n is the number of parameters and m is the dimension of the unit space occupied by the parameters. The relevant IRS vehicle parameters, along with their primary unit dimensions, are

$$\begin{aligned} m &= \text{kg} = [M] \\ V &= \text{m/s} = \left[\frac{Le}{T}\right] \\ Y &= L = L_1 = L_2 = [Le] \\ C_{\alpha f} &= C_{\alpha r} = \left[\frac{\text{kg}\cdot\text{m}}{\text{s}^2}\right] = \left[\frac{MLe}{T^2}\right] \\ I_z &= [\text{kg}\cdot\text{m}^2] = [MLe^2]. \end{aligned} \tag{12}$$

Note that the angles such as the steer angle and slip angle are unitless and, thus, form their own Pi groups. It is clear that the basic unit dimensions are mass, length, and time. Thus, there are three primary dimensions in the unit space, abbreviated M, Le, and T with eight parameters in question. If we choose m, V, and L as repeating parameters, we can express the remaining five parameters as dimensionless groups, to create five additional Pi groups. First, a dimensional equation is formed in powers of the repeating parameters

$$\begin{aligned} C_{\alpha f}\cdot m^a \cdot V^b \cdot L^c &= \left[\frac{MLe}{T^2}\right]\cdot[M]^a \cdot \left[\frac{Le}{T}\right]^b \cdot [Le]^c \\ &= [MLeT]^0. \end{aligned} \tag{13}$$

Equating the powers, three equations are obtained

$$\begin{array}{ll} \text{mass} & 1+a=0 \\ \text{time} & -2-b=0 \\ \text{length} & 1+b+c=0. \end{array} \tag{14}$$

Solving the equations gives $a = -1$, $b = -2$, and $c = 1$. Hence, the first Pi group is $C_{\alpha f}L/mV^2$. Solving for the second Pi group

$$\begin{aligned} I_z \cdot m^a \cdot V^b \cdot L^c &= [MLe^2]\cdot[M]^a \cdot \left[\frac{Le}{T}\right]^b \cdot [Le]^c \\ &= [MLeT]^0. \end{aligned} \tag{15}$$

Equating the powers, three equations are obtained

$$\begin{array}{ll} \text{mass} & 1+a=0 \\ \text{time} & -b=0 \\ \text{length} & 2+b+c=0. \end{array} \tag{16}$$

Solving the equations gives $a=-1$, $b=0$, and $c=-2$. Therefore, the second Pi group is I_z/mL^2. A summary of all the Pi groups is

$$\begin{aligned} \Pi_1 &= \frac{L_1}{L} \\ \Pi_2 &= \frac{L_2}{L} \\ \Pi_3 &= \frac{C_{\alpha f}L}{mV^2} \\ \Pi_4 &= \frac{C_{\alpha r}L}{mV^2} \\ \Pi_5 &= \frac{Iz}{mL^2}. \end{aligned} \tag{17}$$

The Buckingham Pi theorem states that if two dynamic systems are described by the same differential equations, then the solution to these differential equations will be the same if the Pi groups are the same. This becomes clear during nondimensionalization of the governing differential equations.

To determine the validity of the use of scaled vehicles on the IRS, originally the pole locations of the scale vehicle were compared to the full-sized vehicles [10]. These pole locations are determined by the eigenvalues of the "A" matrix for the bicycle model in (2). Not including the double integrator, these open-loop eigenvalues are the solution to the equation

$$\begin{aligned} s^2 + \left(\frac{1}{mV}(C_{\alpha f}+C_{\alpha r}) + \frac{1}{I_z V}(C_{\alpha f}L_1^2 + C_{\alpha r}L_2^2)\right)s \\ + C_{\alpha f}C_{\alpha r}\frac{L^2}{I_z m V^2} - \frac{1}{I_z}(L_1 C_{\alpha f} - L_2 C_{\alpha r}) = 0. \end{aligned} \tag{18}$$

Note that the Laplace variable s has units of (s^{-1}), so we may make a scale transformation to nondimensional coordinates

$$\begin{aligned} &\frac{V^2}{L^2}s*^2 + \frac{V}{L}\left(\frac{1}{mV}(C_{\alpha f}+C_{\alpha r}) + \frac{1}{I_z V}(C_{\alpha f}L_1^2 + C_{\alpha r}L_2^2)\right)s* \\ &\quad + C_{\alpha f}C_{\alpha r}\frac{L^2}{I_z m V^2} - \frac{1}{I_z}(L_1 C_{\alpha f} - L_2 C_{\alpha r}) = 0 \end{aligned} \tag{19}$$

$$\begin{aligned} \Rightarrow\ & s*^2 + \left(\left(\frac{C_{\alpha f}L}{mV^2} + \frac{C_{\alpha r}L}{mV^2}\right) + \frac{mL^2}{I_z}\right. \\ &\left. \cdot \left(\left(\frac{L_1}{L}\right)^2 \frac{C_{\alpha f}L}{mV^2} + \left(\frac{L_2}{L}\right)^2 \frac{C_{\alpha r}L}{mV^2}\right)\right)s* \\ &+ \frac{C_{\alpha f}L}{mV^2}\frac{C_{\alpha r}L}{mV^2}\frac{mL^2}{I_z} - \frac{mL^2}{I_z}\left(\frac{L_1}{L}\frac{C_{\alpha f}L}{mV^2} - \frac{L_2}{L}\frac{C_{\alpha r}L}{mV^2}\right) \\ &= 0 \end{aligned} \tag{20}$$

$$\begin{aligned} \Rightarrow\ & s*^2 + \left((\Pi_3+\Pi_4) + \frac{1}{\Pi_5}(\Pi_1^2\Pi_3 + \Pi_2^2\Pi_4)\right)s* \\ &+ \frac{1}{\Pi_5}(\Pi_3\Pi_4 - \Pi_1\Pi_3 + \Pi_2\Pi_4) = 0. \end{aligned} \tag{21}$$

Clearly, if the Pi groups agree between two systems governed by the bicycle model, then the normalized pole locations will be the same and this will indicate a high degree of dynamic similitude between the two systems. However, the converse is not true. Identical pole locations can map to different Pi groups. Therefore, the Pi group matching is a more rigorous test of dynamic similitude than just considering the system poles. To test this concept, pole locations and Pi groups were compiled for full-sized and IRS-scale vehicles.

TABLE II
DYNAMIC SIMILITUDE COMPARISON

	Vehicle #2	Avg. Full Size
Speed (m/s / mph)	3/6.52	23.8/51.8
Poles	0,0,-4.8+/- 3.5j	0,0,-4.6+/- 3.3j
Pi 1	0.4229	0.4203
Pi 2	-0.5771	-0.5797
Pi 3*	0.2750	0.2750
Pi 4*	0.2750	0.2622
Pi 5	0.2771	0.2593

*These two values can be matched by varying car speed

The average values of vehicle parameters were taken for four different vehicles. Two of these were a full size and compact sedan given in [15]. A third was a 1986 Pontiac 6000STE sedan from the California PATH program [16], and the final set of vehicle parameters were for a Ford Taurus [17]. To summarize the results shown in Table II, analysis shows experimentally and theoretically that there can be good agreement between scale and full-sized vehicle dynamics. To get the proper match between scale and full-size vehicles may involve adjustments of vehicle parameters. For example, in Table II, the inertia of the scaled vehicle was tuned to match the Pi groups by adding and distributing weight to the front and rear of the vehicle. Given the variability of different vehicles' dynamics, an exact match should not be sought. However, the previous analysis should indicate that the dynamics of the IRS-scaled vehicles are similar enough to those of actual vehicles to be useful for controller testing. Algorithms that are deemed successful could then be scaled up to actual full-size tests. It should also be noted that the dynamic similitude results studied so far are for vehicles operating within the linear range of their dynamics. Further investigation is necessary to determine whether or not the dynamic similitude holds in the nonlinear regions of dynamics, particularly tire dynamics at large values of slip or slip angle.

IV. VEHICLE CONTROL: DRIVER-ASSISTED CONTROL (DAC)

The vehicle control scenario examined here with the IRS is DAC. DAC can be used to provide stability and performance, while still allowing the driver to dictate the path of the vehicle, by assisting the driver in her/his directional control of the vehicle. Parameters such as yaw angle, yaw rate, lateral velocity, and lateral acceleration would be sensed or estimated to provide the control with the necessary information to achieve desired transient and steady-state performance based on the driver's input to the vehicle.

The motivation for the DAC controller is to give the driver a "tunable" vehicle in terms of its handling performance. For this investigation, the DAC was implemented on a vehicle by using the rear wheels as the control input. As illustrated in Fig. 12, this still allows the driver to steer the vehicle's front wheels

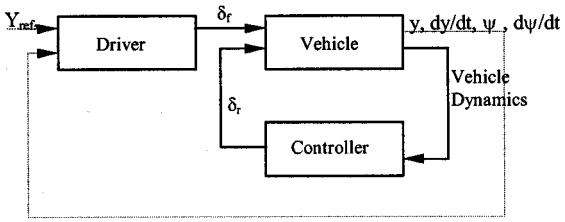

Fig. 12. DAC schematic.

in a customary open-loop fashion. A failure detection method can also be used to lock the rear wheels at zero position if the control becomes unstable for some reason. All of these features are advantages because they utilize the rear wheels as input to alter the dynamic response of the vehicle while still allowing the driver to dictate the vehicle path.

There is a wealth of literature on lateral vehicle dynamics modeling and automatic 2WS and 4WS control designs as detailed in [6]. Additionally, there have been many studies done on 4WS approaches to change the vehicle's dynamics [18]–[22]. Typically, the strategies associated with 4WS can be categorized into feedforward and feedback approaches [21]. The feedforward approaches usually set the rear steer angles to be a function of the front steer angles, for example a pure gain

$$\delta_r = K_{\text{steer}}(V) \cdot \delta_f. \tag{22}$$

In this case, the goal of the controller is simply to minimize the steady-state sideslip angle of the vehicle using a predefined gain as a function of the vehicle speed. Other feedforward approaches use a filtered or delayed value

$$\delta_r = \frac{K_1 s + K_0}{\tau s + 1} \cdot \delta_f \tag{23}$$

where the values of the constants may be determined via linear optimal control [23]. The goal of the filtering is usually to alleviate the reverse vehicle sideslip during transient responses. There have been several feedback approaches to 4WS as well. The simplest ones have been straightforward extensions of the feedforward strategies where the vehicle yaw rate was fed back to the rear wheels

$$\delta_r = K_{\text{steer}} \cdot \delta_f + K_{\text{yaw}} \cdot \dot{\psi}. \tag{24}$$

The goal of the yaw rate feedback is to utilize a measurable variable to provide additional sideslip minimization at higher vehicle speeds. Some investigators considered full state feedback, but lateral velocity states are inherently difficult to determine. Relatively few of the previous investigations attempt to actually make the vehicle behave as if it had a different set of dynamics through feedback.

To construct the DAC, a model reference controller (MRC) strategy [24] will be used along with a modification based on rejection of known disturbance dynamics. Model reference (model following) controller design is a method by which desired closed-loop characteristics can be introduced into a system, i.e., a pole placement method. The basic MRC approach has a systematic method for the controller design. Assume the plant can be modeled as a ratio of two linear polynomials

$$\frac{Y(s)}{U(s)} = G(s) = \frac{B(s)}{A(s)}. \tag{25}$$

The polynomial A is assumed to be monic and of degree n. B can be nonmonic and of degree less than or equal to n. It is also assumed that the polynomials are relatively prime, i.e., they have no common factors. The desired closed-loop performance is

$$\frac{Y(s)}{U_c(s)} = G_m(s) = \frac{B_m(s)}{A_m(s)}. \tag{26}$$

The control law is given by

$$Ru(t) = Tu_c(t) - Sy(t) \tag{27}$$

where R, S, and T are polynomials in the Laplace operator s. The controller consists of a feedforward term (T/R) and a feedback term (S/R). The idea behind the controller is to cancel out the unwanted plant dynamics and replace them with the designer's own desired dynamics.

To design the polynomials R, S, and T, it is necessary to take a closer look at the closed-loop system in question

$$y(t) = \frac{BT}{AR + BS} u_c(t). \tag{28}$$

To have the closed-loop system performance be identical to the desired reference, the closed-loop polynomials and the reference model must be identical

$$\frac{BT}{AR + BS} = \frac{B_m}{A_m}. \tag{29}$$

Equation (29) implies pole/zero cancellations occur between BT and $AR + BS$. Then, if B is separated into stable and well-damped zeros (B^+) and unstable or poorly damped zeros (B^-), B^- must be a factor of B_m. This also means that B^+ is canceled, so it must be a factor of $AR + BS$. A_m must also be a factor of $AR + BS$ since it is the desired model characteristic polynomial. Therefore, $AR + BS$ must include A_m, B^+, and what is called the observer polynomial, A_o, for causality conditions. Finally, since A and B are relatively prime and B^+ is a factor of B and $AR + BS$, B^+ must also be a factor of R. R can then be factored into

$$R = R' B^+. \tag{30}$$

To solve for R, S, and T, the logical steps just followed reduce the closed-loop polynomial matching to

$$A \cdot R' - B^- \cdot S = A_0 \cdot A_m \tag{31}$$

$$T = A_0 \cdot B'_m \tag{32}$$

where $B_m = B^- B'_m$.

As long as A and B are relatively prime, (31) has a solution. For R, S, and T to be causal, the following conditions must be satisfied:

$$\begin{aligned} &\text{degree } (S) \leq \text{degree } (R) \\ &\text{degree } (T) \leq \text{degree } (R). \end{aligned} \tag{33}$$

A more detailed discussion of this topic, including minimum degree solutions, is given in [24].

To tailor the basic MRC approach for the DAC, the driver front steer input will act as a reference command to the MRC of the rear steer model while simultaneously acting as a known output disturbance to the vehicle's yaw rate. Assume the same reference model from (26), but the plant dynamics of (25) are now given as

$$y = \frac{B(s)}{A(s)}u + \underbrace{\Delta}_{\text{disturbance}}. \tag{34}$$

Assume that the disturbance Δ can be separated into two parts: known dynamics and unknown disturbances. Assuming a rational, causal transfer function representation for the disturbance dynamics gives

$$\Delta(s) = \underbrace{\frac{B_d(s)}{A_d(s)}}_{\substack{\text{known}\\ \text{dynamics}}}\gamma(s) + \underbrace{\nu(s)}_{\substack{\text{unknown}\\ \text{disturbance}}}. \tag{35}$$

The term γ is defined as the disturbance generator for the known disturbance. The unknown disturbance term v contains both unmodeled dynamics of the system as well as external disturbances (e.g., wind) that are not known. Suppressing the Laplace operator for convenience, (34) can be rewritten as

$$A_dAy = A_dBu + AB_d\gamma + AA_d\nu. \tag{36}$$

The new control signal differs in structure from (27) by the inclusion of a disturbance compensation term below.

$$u = \frac{T}{R}u_c - \frac{S}{R}y + \underbrace{\frac{B_c}{A_c}}_{\substack{\text{disturbance}\\ \text{compensator}\\ \text{polynomial}}} \cdot \underbrace{\gamma}_{\substack{\text{known}\\ \text{disturbance}\\ \text{generator}}}. \tag{37}$$

Substituting (37) into (36) gives

$$\frac{A_d(AR+BS)}{R}y = \frac{A_dBT}{R}u_c + \left(\frac{A_dBB_c}{A_c} + AB_d\right)\gamma + AA_dv \tag{38}$$

$$\Rightarrow y = \frac{BT}{AR+BS}u_c + \frac{R}{A_d(AR+BS)} \cdot \left(\frac{A_dBB_c + AA_cB_d}{A_c}\right)\gamma + \frac{AR}{(AR+BS)}v. \tag{39}$$

The desired result is for the known disturbance to have no effect on the output of the closed-loop model matching system. Considering (39), to achieve this requires that the polynomial in front of the disturbance generator γ be canceled

$$A_dBB_c + AA_cB_d = 0 \Rightarrow \frac{B_c}{A_c} = -\frac{AB_d}{A_dB}. \tag{40}$$

Considering (37) again, while using the disturbance compensator identified in (40), and simplifying for the input u results in

$$u = \frac{T}{R}u_c - \frac{S}{R}\left(\frac{BT}{AR+BS}u_c + \frac{AR}{(AR+BS)}v\right) + \frac{AB_d}{A_dB}\gamma \tag{41}$$

$$\Rightarrow u = \frac{AT}{AR+BS}u_c - \frac{AS}{(AR+BS)}v - \frac{AB_d}{A_dB}\gamma. \tag{42}$$

For the DAC controller, the reference model G_m represents the desired response from the driver's front steer input to the vehicle's yaw rate

$$y_{\text{des}} = \dot{\psi}_{\text{des}} = G_m\delta_f = \frac{B_m}{A_m}\delta_f. \tag{43}$$

Therefore, the command input u_c is actually the driver steer command δ_f.

$$u = \frac{AT}{AR+BS}\delta_f - \frac{AB_d}{A_dB}\gamma - \frac{AS}{(AR+BS)}v. \tag{44}$$

However, the disturbance generator is also the front steer angle command $\gamma = \delta_f$ since it is the driver's steering that causes uncontrolled changes in the yaw rate. Consequently, the input can be redefined as

$$u = \underbrace{\left(\frac{AT}{(AR+BS)} - \frac{AB_d}{A_dB}\right)\delta_f}_{\text{feedforward}} - \underbrace{\frac{AS}{(AR+BS)}v}_{\text{feedback}} \tag{45}$$

where the disturbance polynomials A_d, B_d are the denominator and numerator polynomials for the transfer function from front steer command to yaw rate. As is evident, (45) represents a two-degrees–of-freedom (2DOF) controller with both a feedforward and feedback component. Ideally, the better the models for the front and rear steer transfer functions, the larger the relative activity of the feedforward portion of the controller. Also, it should be noted that there are no causality problems associated with the formulation of the known disturbance compensator since the transfer functions from front steer command to yaw rate and rear steer command to yaw rate both have the same order and relative degree.

The uniqueness of this model reference approach is that the effect of the driver's front steer input on the vehicle yaw rate is formulated as an output disturbance which should be rejected by the controller governing the rear wheels. Obviously, the front steer will be aiding in the output yaw rate tracking of the desired reference model for much of the time. Therefore, the controller's rear wheel steering will add only that incremental steer effort which is deemed necessary. Since the steady-state gain of the yaw rate from front steer input is a function of the vehicle's understeer gradient [11], the choice of both transient and steady-state reference model performance completely dictates the vehicle's understeer characteristics.

The open-loop transfer functions for front and rear steering are obtained by combining the steering actuator dynamics with the bicycle model dynamics developed previously. Slightly adjusting the vehicle dynamics transfer function from the

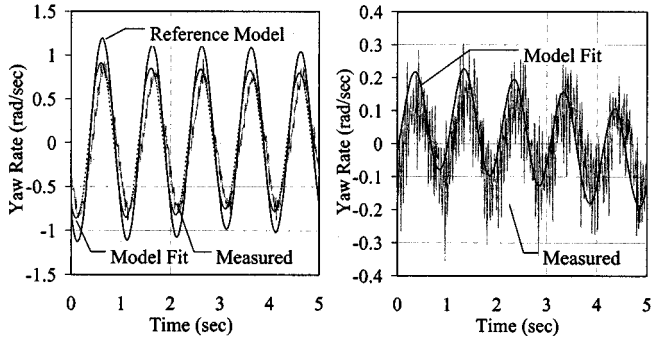

Fig. 13. Reference model versus experimental yaw rate for front (left) and rear (right) steering.

frequency-domain fit of Fig. 11 to incorporate some of the system nonlinearities and time delay, the resulting transfer functions for 3.0 m/s velocity are

$$\frac{\dot{\psi}(s)}{V_f(s)} = \frac{B_d(s)}{A_d(s)} = \underbrace{\frac{3510}{s^2+60.5s+1764}}_{\text{steer servo dynamics}} \cdot \underbrace{\frac{42.7s+752}{s^2+21s+170.6}}_{\text{vehicle dynamics}} \tag{46}$$

$$\frac{\dot{\psi}(s)}{V_r(s)} = \frac{B(s)}{A(s)} = \underbrace{\frac{751}{s^2+36s+625}}_{\text{steer servo dynamics}} \cdot \underbrace{\frac{-131s-752}{s^2+21s+170.6}}_{\text{vehicle dynamics}} \tag{47}$$

where the yaw rate is in degrees per second and the input is in volts.

The time responses of Fig. 13 support the frequency response of Fig. 11 to justify a good model fit. The reference model was chosen to give a fast, stable, transient response by increasing the damping and the dc gain of the bicycle model. The damping improves vehicle stability by preventing overshoot for transient maneuvers, while the dc gain is included to make the vehicle seem more responsive to slow, steady-state steering inputs. Significant pole movement is intentionally avoided to prevent driver discomfort and actuator saturation. In the investigation presented here, inclusion of the actuator dynamics in the reference model was found to be important. The controller is physically unable to change the actuator dynamics; however, inclusion of these dynamics is required for good performance

$$\frac{B_m(s)}{A_m(s)} = \underbrace{\frac{3510}{s^2+60.5s+1764}}_{\text{steer servo dynamics}} \cdot \underbrace{\frac{56.4s+1128}{s^2+26s+170.6}}_{\text{desired dynamics}}. \tag{48}$$

The resulting MRC polynomials are given as

$$R(s) = 0.39 \cdot s^3 + 35.9 \cdot s^2 + 1579 \cdot s + 7958 \tag{49}$$

$$S(s) = -0.152 \cdot s^3 - 7.30 \cdot s^2 - 1177 \cdot s - 4089 \tag{50}$$

$$T(s) = -0.786 \cdot s^3 - 60.19 \cdot s^2 - 2147 \cdot s - 25\,160 \tag{51}$$

$$A_o(s) = 1/40^2 \cdot s^2 + 2 \cdot 0.707/40 \cdot s + 1. \tag{52}$$

The front steer commands to control the vehicle's lateral position on the IRS are controlled via a computer as shown in Fig. 1. Fig. 14 shows the output of the reference model and the response of the vehicle with DAC particular input. Without DAC (Fig. 13), the system is operating in the open loop. Clearly, with the DAC the vehicle's yaw degree of freedom behaves much more like the desired reference model.

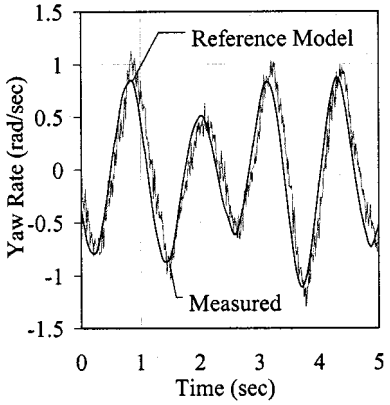

Fig. 14. Reference model versus experimental yaw rate.

Traditionally, controller implementation on full-sized vehicles is often discussed without regard to how the actuator dynamics may interfere with the controller design. To emphasize the importance of these dynamics, the above MRC-based approach was conducted where the actuator dynamics are approximated by a dc gain rather than a transfer function. The frequency responses of the bicycle model without the actuator dynamics are also shown in Figs. 11 and 6. The resulting design polynomials, again for 3.0 m/s velocity, are

$$\frac{\dot{\psi}(s)}{V_f(s)} = \frac{B_d(s)}{A_d(s)} = \underbrace{1.99}_{\substack{\text{steer servo}\\ \text{dynamics}}} \cdot \underbrace{\frac{42.7s+752}{s^2+21s+170.6}}_{\text{vehicle dynamics}} \tag{53}$$

$$\frac{\dot{\psi}(s)}{V_r(s)} = \frac{B(s)}{A(s)} = \underbrace{1.20}_{\substack{\text{steer servo}\\ \text{dynamics}}} \cdot \underbrace{\frac{-131s-752}{s^2+21s+170.6}}_{\text{vehicle dynamics}} \tag{54}$$

$$\frac{B_m(s)}{A_m(s)} = \underbrace{1.99}_{\substack{\text{steer servo}\\ \text{dynamics}}} \cdot \underbrace{\frac{56.4s+1128}{s^2+26s+170.6}}_{\text{desired dynamics}} \tag{55}$$

and the resulting MRC polynomials are given as

$$R(s) = s + 5.74 \tag{56}$$

$$S(s) = -0.0325 \cdot s \tag{57}$$

$$T(s) = -0.713 \cdot s - 14.26 \tag{58}$$

$$A_o(s) = 1. \tag{59}$$

The resulting controller implementation is shown in Fig. 15. As can be seen in comparing Figs. 14 and 15, the inclusion of the steer actuator dynamics has a significant effect on the output tracking ability.

For comparison of the MRC-based DAC approach, a simple proportional control was applied to the error between the reference model yaw rate and the actual vehicle yaw rate

$$\delta_r = K_p(\dot{\psi}_{\text{reference}} - \dot{\psi}_{\text{measured}}). \tag{60}$$

The proportional gain was selected to match the dc gain of the feedback term of the MRC design: -0.05 [volts/(rad/s)]. Fig. 16 gives a comparison between the reference model and the actual

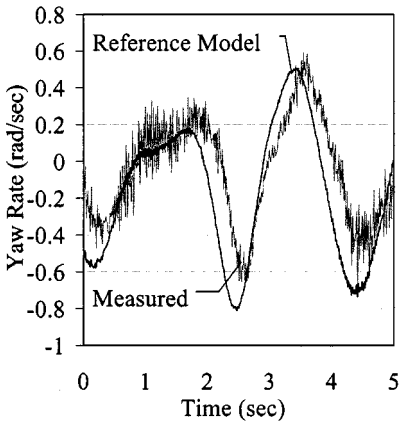

Fig. 15. DAC yaw rate without actuator dynamics accounted for.

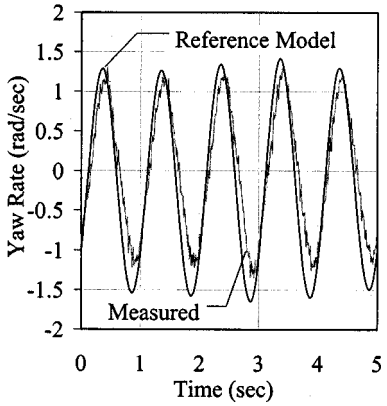

Fig. 16. P-control on yaw rate feedback ($K_p = 0.05$).

vehicle yaw rate for a vehicle performing a sinusoidal steer front steer input. As seen in the figure, the system under proportional (P) control does a poor job of tracking the reference model's desired output. A comparison of Figs. 14 and 16 indicates that the DAC approach is better at achieving satisfactory yaw rate control than a simple proportional feedback approach.

The MRC-based DAC relies on a fairly accurate model of the vehicle. However the vehicle's dynamics may change significantly with velocity. Sensitivity tests were conducted where the vehicle is operated outside the velocity range of controller design. Using the design speed of 3.0 m/s, the controller was operated faster than the design. Fig. 17 demonstrates a serious degradation in controller performance when operated at off-design speeds. In an effort to make the control approach feasible across a range of parameter variations, a continuous-time recursive least-squares adaptive estimator was combined with the original DAC in [25]. The estimator operated on a reduced-order model of the vehicle. The approach was shown to be successful for the experimental IRS system and was able to account for vehicle parameter changes due to increased speed. However, the proper parameter convergence for the front and rear steer transfer functions required more persistence of excitation (PE) than would probably be available in an actual vehicle. In a nominal driving condition, which consists of relatively small driver

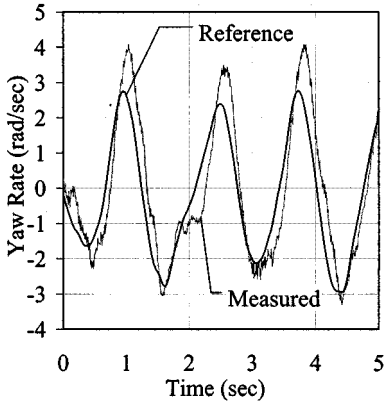

Fig. 17. DAC control at 3.5 m/s.

input, the identification scheme may not obtain enough PE to get convergence to the actual parameters. Consequently, a velocity scheduled control approach based on offline system identification may be more realistic in practice and is the avenue of ongoing IRS research efforts.

V. Conclusions

The IRS has been introduced and shown to be a viable testbed for vehicle control applications. Various components and subsystems have been introduced and models developed for each. Using nondimensional analysis, the models developed for the scaled vehicles operating on the IRS are shown to be dynamically very similar to those of actual vehicles within the range of linear dynamics considered here. It is felt that this validates controller design efforts that may be tried out on the IRS. The IRS is flexible, inexpensive, easily reconfigurable, and safe enough to attempt several controller strategies. In this work we demonstrate its use in evaluating a yaw-rate control scheme termed DAC which aims to change the vehicle dynamics from the driver's point of view. For these investigations, the actuator dynamics turned out to be an important part of the vehicle system that should not be ignored during the controller design in obtaining the best performance. Robustness studies were done to demonstrate the sensitivity of the DAC to system parameters and suggest methods for overcoming this.

References

[1] M. Barron and W. F. Powers, "The role of electronic controls for future automotive mechatronic systems," *IEEE/ASME Trans. Mechatron.*, vol. 1, pp. 80–88, Mar. 1996.
[2] J. Ackermann, "Robust control prevents car skidding," *IEEE Contr. Syst. Mag.*, vol. 17, pp. 23–31, June 1997.
[3] D. Hrovat, "Survey of advanced suspension developments and related optimal control applications," *Automatica*, vol. 33, no. 10, pp. 1781–1817, 1997.
[4] M. Abe, "On advanced chassis control technology for vehicle handling and active safety," in *Proc. AVEC'96*, Aachen, Germany, June 1996, pp. 1–12.
[5] A. Straub, "DSC (dynamic stability control) in BMW 7 series cars," in *Proc. AVEC'96*, Aachen, Germany, June 1996, pp. 547–557.
[6] M. Tomizuka and J. K. Hedrick, "Advanced control methods for automotive applications," *Vehicle Syst. Dynam.*, vol. 24, pp. 449–468, 1995.
[7] S. Shladover, "Review of the state of development of advanced vehicle control systems (AVCS)," *Vehicle Syst. Dynam.*, vol. 24, pp. 551–595, 1995.

[8] M. Sampei, T. Tamura, T. Kobayashi, and N. Shibui, "Arbitrary path tracking control of articulated vehicles using nonlinear control theory," *IEEE Trans. Contr. Syst. Technol.*, vol. 3, pp. 125–131, Mar. 1995.
[9] N. Matsumoto and M. Tomizuka, "Vehicle lateral velocity and yaw rate control with two independent control inputs," *ASME J. Dynam. Syst., Meas., Contr.*, vol. 114, pp. 606–613, Dec. 1992.
[10] S. Brennan, M. DePoorter, and A. Alleyne, "The Illinois roadway simulator—A hardware-in-the-loop testbed for vehicle dynamics and control," in *Proc. 1998 American Control Conf.*, Philadelphia, PA, June 1998, pp. 493–497.
[11] G. Genta, *Motor Vehicle Dynamics: Modeling and Simulation*. Singapore: World Scientific, 1997.
[12] H. Peng and M. Tomizuka, "Preview control for vehicle lateral guidance in highway automation," *ASME J. Dynam. Syst., Meas., Contr.*, vol. 115, pp. 679–686, Dec. 1993.
[13] T. S. Stombaugh, "Automatic guidance of agricultural vehicles at higher speeds," Ph.D. dissertation, Dep. Agri. Eng., Univ. Illinois, Urbana-Champaign, IL, 1998.
[14] E. Buckingham, "On physically similar systems: Illustrations of the use of dimensional equations," *Phys. Rev.*, vol. 4, pp. 345–76, 1914.
[15] L. D. Reid, E. N. Solowka, and A. M. Billing, "A systematic study of driver steering behavior," *Ergonomics*, vol. 24, no. 1, pp. 447–462, 1981.
[16] J. Guldner, H. S. Tan, and S. Patwardhan, "Analysis of automatic steering control for highway vehicles with look-down lateral reference systems," *Vehicle Syst. Dynam.*, vol. 26, pp. 243–269, 1996.
[17] T. Pillutti, G. Ulsoy, and D. Hrovat, "Vehicle steering intervention through differential braking," in *Proc. 1995 American Control Conf.*, Seattle, WA, June 1995, pp. 1667–1671.
[18] M. Yamamoto, "Active control strategy for improved handling and stability," SAE, Technical Paper Series, no. 911902, 1991.
[19] J. Sato, H. Kawai, M. Isikawa, H. Iwata, and S. Koike, "Development for four wheel steering system using yaw rate feedback control," SAE, Technical Paper Series, no. 911922, 1991.
[20] Y. Lin, "Improved vehicle handling performance by a closed-loop 4WS driving controller," SAE, Technical Paper Series, no. 921604, 1992.
[21] H. Inoue and F. Sugasawa, "Comparison of feedforward and feedback control for 4WS," *Vehicle Syst. Dynam.*, vol. 22, pp. 425–436, 1993.
[22] Y. Furukawa and M. Abe, "Advanced chassis control systems for vehicle handling and active safety," *Vehicle Syst. Dynam.*, vol. 28, pp. 59–86, 1997.
[23] Y. H. Cho and J. Kim, "Design of optimal four-wheel steering system," *Vehicle Syst. Dynam.*, vol. 24, pp. 661–682, 1995.
[24] K. J. Astrom and B. Wittenmark, *Computer Controlled Systems: Theory and Design*. Englewood Cliffs, NJ: Prentice-Hall, 1997.
[25] M. DePoorter, S. Brennan, and A. Alleyne, "Driver assisted control strategies: Theory and experiment," in *Proc. 1998 ASME IMECE*, vol. DSC-63, Anaheim, CA, Nov. 1998, pp. 215–222.

Sean Brennan received the B.S.M.E. and B.S. Physics degrees from New Mexico State University, Las Cruces, in 1997, graduating first in both the College of Engineering and the College of Physics, and the M.S. degree in mechanical engineering in 1999 from the University of Illinois, Urbana-Champaign, where he is currently working toward the Ph.D. degree in mechanical engineering with support from a National Science Foundation Graduate Fellowship.

His interests are in robust control of dimensionally varying systems, coordinated control, and general nonlinear control.

Andrew Alleyne (M'95) received the B.S.E. degree (*magna cum laude*) in mechanical and aerospace engineering from Princeton University, Princeton, NJ, and the M.S. and Ph.D. degrees from the University of California at Berkeley, in 1989, 1992, and 1994, respectively.

In 1994, he joined the Mechanical and Industrial Engineering Department, University of Illinois, Urbana-Champaign, where he is currently an Assistant Professor. His areas of interest include the application of nonlinear control and adaptive control to vehicles, manufacturing systems, vibration control, and fluid power systems.

Dr. Alleyne was the recipient of a National Science Foundation CAREER Award in 1996.